Università degli Studi di Bologna

FACOLTA' DI INGEGNERIA

Corso di Dottorato in
ING-IND/13: MECCANICA APPLICATA ALLE MACCHINE
Ciclo XXII

An New Energetic Approach to the Modeling of Human Joint Kinematics: Application to the Ankle

Tesi di Dottorato di:
Ing. Michele Conconi

Coordinatore:
Chiar.mo Prof. Vincenzo Parenti Castelli

Tutore:
Chiar.mo Prof. Vincenzo Parenti Castelli

Anno Accademico 2009-2010

Abstract

The objective of this dissertation is to develop and test a predictive model for the passive kinematics of human joints based on the energy minimization principle. To pursue this goal, the tibio-talar joint is chosen as a reference joint, for the reduced number of bones involved and its simplicity, if compared with other sinovial joints such as the knee or the wrist.

Starting from the knowledge of the articular surface shapes, the spatial trajectory of passive motion is obtained as the envelop of joint configurations that maximize the surfaces congruence. An increase in joint congruence corresponds to an improved capability of distributing an applied load, allowing the joint to attain a better strength with less material. Thus, joint congruence maximization is a simple geometric way to capture the idea of joint energy minimization.

The results obtained are validated against in vitro measured trajectories. Preliminary comparison provide strong support for the predictions of the theoretical model.

An New Energetic Approach to the Modeling of Human Joint Kinematics: Application to the Ankle

Michele Conconi

May 18, 2010

Contents

Chapter 1

Introduction

Diarthrodial or synovial joints are the most movable ones in the human body. Joints of this kind are for example the hip, the knee, the ankle and the wrist. They are involved in all daily activities and subjected to a big variety of diseases and injuries. Due to their fundamental role, an impressive and increasing effort is devoted to their study. In particular, modeling their normal behavior is the fundamental first step for assessing their pathologies and consequently making possible treatments definition, surgical planning and design of prostheses. It is possible to approach the modeling of human joint in many different ways, nevertheless we may identify two major families: a simultaneous approach and a sequential approach. On the former are grouped those models that consider at the same time all the biological structures composing the joint [2, 22, 1, 13, 20, 25, 8] typically representing them by means of lumped and/or distributed parameters, such as linear and non-linear elastic and dumping elements. Although computationally demanding, these models are suitable to simulate the overall dynamic behavior of the joint and they allow to evaluate data which could not be directly recorded in an experimental session, such as the forces exerted by muscles. The main drawback of this approach is that it is highly dependent on the data employed for the tuning of its parameters. Indeed, due to the great complexity of human joints and to the highly non-linear interactions among their structures, this tuning change dramatically with the task used as comparison. This lack of generality makes impossible any forecast on the joint behavior outside of the task for which the model has been optimized.

On the other side, the sequential approach try to explain the nature of the joint structures and their interactions rather than investigate a specific problem. The analysis is subdivided into different steps [10, 24]. Each step studies few anatomical structures under hypotheses that allow to neglect the influence of the others joint elements, making thus possible to isolate and better understand their role in the behavior of the joint. Each further step exploits the knowledge gained in the previous one; new features are added and the hypotheses are made less restrictive, increasing the complexity and the generality of the model. Such an approach is less suitable to directly asses the overall behavior of a joint under precise condi-

tions but it makes it possible to realize a more general model, since the informations collected in this way possess a global validity. To develop a joint model via a sequential approach, the first step is to isolate and study its passive structures. Many works in the literature set on this path. Wilson and O'Connor [32, 31] first proposed a parallel mechanism kinematically equivalent to the knee to separate the position form the static analysis. Later, Parenti-Castelli and Di Gregorio [21, 7] and Sancisi and Parenti-Castelli [23] improved this model, also extending it to the ankle [6, 9]. All these works reach the goal of enlighten the role of passive structure by modeling the motion under virtually unloaded conditions, the so-called *passive motion*. This ideal motion can be obtained as a sequence of position of neutral equilibrium [32, 30]. In the absence of external perturbations indeed, a joint should move along a path determined solely by the constraints imposed by the passive structures, namely the articular surfaces and the ligaments.

It would be possible to go further on the sequential approach and isolate the role played by solely the articular surfaces once a relation was establish between their shape and the passive kinematics. An help in this direction comes from the work of the German anatomist Julius Wolff [33, 11], who stated a principle, known as *Wolff's Law*, according to which bones remodel themselves adapting optimally to change in stress, attaining maximum strength with minimum material.

Wolff noticed that the misalignment in fractured long bones healed with an angulations tend to vanish in time. Rather than progressively weaken the bone structure, the initial bending stress results in a modeling and remodeling, with new bone growth on the concave compressed side and bone resorption on the convex tensioned side. If the patient were young enough, the bone ultimately grown straight. We may resume such a principle as an alternative formulation of a minimum energy principle: a more uniform stress distribution allows a better use the overall structure of the bone, requiring less material for resist to the same load, thus resulting in a save of energy from a biological view point (see Section 2.2).

A first attempt to develop a wrist kinematic model relaying only on the information collected for the shape of the articular surfaces was made by Sirkett et al. [27]. They assumed that this joint moves so as to maximize contact areas among the carpal bones, therefore minimizing peak local loading. As pointed out by Marai [18], however, the Sirkett's model was only able to correctly predict wrist kinematics in a very narrow range of motion. An explanation may be found considering that they try to model a general motion. However, out of the passive (unloaded) one, the respect of the Wolff's Law is no longer guaranteed since deformations may take place, possibly guiding the relative motion of the bones on a path where the redistribution of the load is no longer the most uniform. Also, in such a condition the contribution of the ligaments to determine the joint kinematics is no longer negligible.

It is worth to underline that there is at least one load condition that can be theoretically predicted by means of the Wolff's principle, i.e. the one according to whom the surface are shaped. In this case the load drives the joint on a path that is in agreement with the passive constraints, thus the guided and passive motion in

this case coincide.

The idea that the Wolff's Principle may be used for modeling the passive motion implies that the latter may be defined as a minimum energy path. A further confirmation to this idea comes from previous models of the passive motion for the knee and the ankle (see [23, 9] for recent contributions). These relay on the experimental evidence that during such a motion some of the ligaments remain unextended. We can read it as a minimization of the energy, since keeping the length of the ligaments constant minimizes the joint elastic potential.

Once that the model is set under the proper boundary condition, a measure on how a configuration matches the minimum energy principle has still to be provide. Since no load can be introduced into the model, the capability of transmitting and redistributing a system of forces has to be geometrically defined.

Sirkett et al. tried to do that by estimating the contact area. They considered in contact each portion of the surfaces of coupled bones closer to each other than a prescribed threshold. Anyway, more important than the total amount of this area it is how the same is distributed, as it will be shown in the chapter 2.3.

The objective of this dissertation is to develop and test a predictive model for the kinematics of human joints based on the energy minimization principle expressed by the Wolff's Law. To pursue this goal, the tibio-talar joint is chosen as a reference joint, for the reduced number of bones involved and its simplicity, if compared with other sinovial joints such as the knee or the wrist. Only the passive motion will be modeled, to ensure the applicability of the Wolff's Law.

This work is organized as follows. Chapter 2 will explain the mechanism at the basis of the osteogenesis, providing further foundation for the model. In Chapter 3 the general anatomy of the ankle will be introduced, together with definition of reference frames employed to express the tibio-talar motion and the procedure to measure it in vitro. A new geometrical measure for the joint congruence will be defined in Section 3.5 to represent the capability of the articulation to redistribute an applied load, thus representing the energy level in the considered joint configuration, while in Section 3.6 the numerical procedure will be developed to reconstruct the passive kinematics exploiting such a measure. This algorithm will be validated against in vitro experimental data of the tibio-talar passive motion in Chapter 4, where the sensitivity analysis will be also carried on, to assess the behavior of the algorithm with the change of its internal parameters. Chapter 5 will present and discuss the limitations of the model. Finally, in Chapter 6 conclusions will be drawn.

Chapter 2

Theoretical foundation of the model

2.1 Wolff's Law: the bone mechanostat

"Bone is a dynamic tissue that is normally renewed through balanced bone resorption and formation processes that are choreographed in space and time. Tight coupling of these processes required to maintain the skeleton, and loss of coupling results in skeletal pathologies. The main actors involved in the bone tissue remodeling are: osteocytes, the putative mechanosensors; osteoblasts that deposit bone matrix; osteoclasts that resorb bone" [4].

The understanding of the mechanisms behind the bones formation and shaping began by 1892 when Julius Wolff realized that mechanical loads can affect bones architecture [33]. He observed that the misalignment of long bones due to incorrect healing from a fracture tends to be spontaneously corrected in young patients. Instead of weaken the bone, the bending produced by the misalignment during the everyday activity results in a modeling and remodeling, with new bone growth on the concave compressed side and bone resorption on the convex tensioned side, bringing the bone structure back to the correct configuration (Fig. 2.1).

The functioning of this mechanism, also called *mechanostat*, is very complex and yet to be fully understood. Each load acting on a bone causes strains in it that generate signals able to activate the action of osteoblasts and osteoclasts. Depending on the intensity of the load the structure of the bone responds in different ways. Where bone strains exceed bone's modeling threshold range (MES_m), modeling can switch on to strengthen to bone structure, whereas when bone strains stay below a lower threshold range (MES_r), disuse-mode remodeling can turn on to reduce whole-bone strength by removing some trabecular and endocortical bone. Thus if E signifies the typical peak strains acting on a bone, then in a healthy subject it will be $MES_r < E < MES_m$. Repeated bone strains cause microscopic fatigue damage in bone. This micro fractures have an operational threshold strain range (the MES_p) that lies above the bone's MES_m. Normally, load bearing bones can

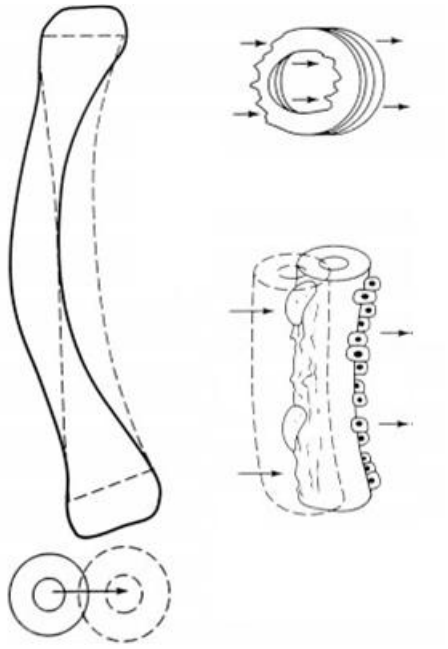

Figure 2.1: The process of realignment due resorption (on the left tensioned side) and formation (on the right compressed side) of bone material.

detect and repair the little damage if there are generated by a stress lower than the MES_p. Strains above the MES_p threshold can cause enough micro damages to escape repair and accumulate, causing pathologic fractures, non traumatic fractures in true osteoporoses and irradiated bone, and stress fractures in athletes. Finally, if the strain exceeds the fracture strength Fx, the bone brakes. Figure 2.2 summarized the bone response to the strain acting on it, while Table 2.1 shows the normal value for the strain threshold in healthy mammals. The horizontal line at the bottom suggests typical peak bone strains from zero on the left, to the fracture strain on the right (Fx), plus the locations of bone's three threshold ranges (MES, MES_m, and MES_p). The dashed outlines suggest the range of variation of bone strength around the average value (dotted line) due to the continuous modeling and remodeling of the bone structure. When strains enter or exceed the MES_m, modeling drifts would begin to increase bone strength. Beyond the MES_p range, woven bone formation usually replaces lamellar bone formation. At the top, DW indicates disuse window; AW, adapted window as in normally adapted young adults; MOW, mild overload window as in healthy growing mammals; and POW, pathologic overload window.

We may summarized the complexity of the mechanostat as follow: nature lets a bone determine its strength by making the relationship between its stiffness and the strain caused by the voluntary mechanical loads on it help to switch its modeling and disusemode remodeling functions on and off.

Before birth, gene expression in utero creates some baseline conditions that

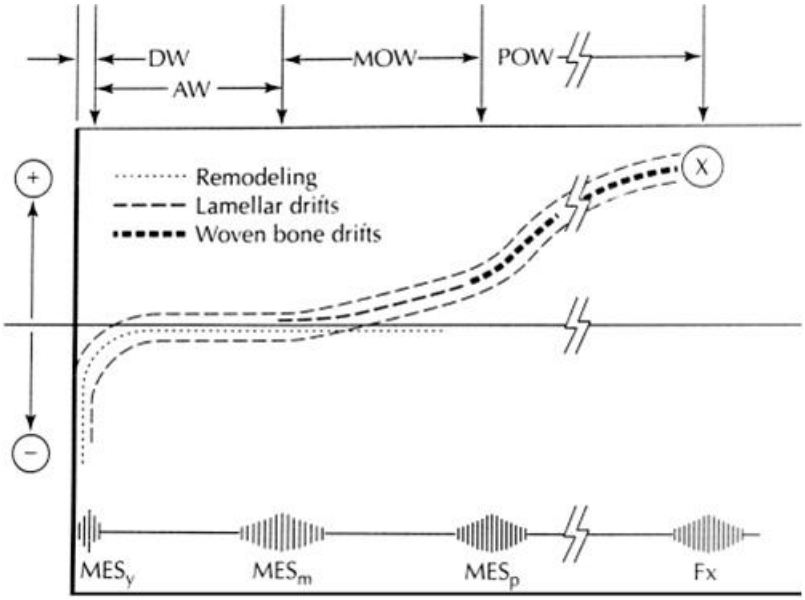

Figure 2.2: The mecahnostat. (reproduced by permission: Frost HM. Strain and other mechanical influences on bone strength and maintenance. Curr Opin Orthop. 1997;8:60-70).

Table 2.1: Bone's thresholds in healthy young-adult mammals.

	MES_f	MES_m	MES_p	Fx
MPa	1-2	20	60	120

include our initial bony anatomy and relationships and the biologic machinery that can adapt bones after birth to mechanical and other challenges so that they can endure these challenges for life.

After birth, bone's mechanostat makes load bearing bones strong enough to keep voluntary mechanical loads from breaking them suddenly or from fatigue. It adapts bone strength to the voluntary mechanical loads acting on it. Finally, it lets the MES_r and MES_m act as criteria for an load bearing bone's acceptable strength relative to the size and kinds of voluntary mechanical loads on it.

2.2 En energetic formulation of the Wolff's Law

From the above description it emerges that the bones, rather than be permanently defined, have to be considered as becoming structures, that are constantly resorbed, rebuild and remodeled. The maintenance of such a structure has therefore a metabolic cost. Under this perspective, it is clear why the growth of the bones may be justify only as response to an environmental request and similarly why, once

this request ceases, part of the bones' structure must be reabsorbed.

In the words of Wolff, bone adapted optimally to changes in stress, attaining maximum strength with minimum material. We can translate the Wolff's principle into an energetic form: the bones adapt themselves to respond to the typical task they are subjected to with the smaller biological cost, i.e. by using the smaller amount of material possible.

Practically speaking, the mechanostat builds new material where the strain is higher, resorbing the bone where unloaded. As a consequence, the final bone structure results evenly loaded, presenting a flat pressure distribution, with the maximum strain always below the bone model threshold MES_m.

This interesting concept constitutes the base for the model developed in this work. Since most of the time a load is transmitted to a bone from a second one coupled with it through a joint, it becomes natural to think that also the design of the articular surfaces should agree with the Wolff's Principle. Furthermore, this should be true not only for one configuration, but along the entire trajectory.

To capture the capability of a given joint configuration to transmit and redistribute a load we turn to a measure of its congruence.

2.3 A measure of the joint congruence as a measure of the joint energy

Joint congruence indicates how well mating surfaces fit together. An increase in it corresponds to a better mating among the articular surfaces and to an improved capability of distributing an applied load. This results in an optimum employ of the bone material. Thus, joint congruence maximization is a simple geometric way to capture the idea of energy minimization.

In the literature it is possible to find different measures for the congruence in a joint (see for instance [5] and [26]), all essentially based on the relative curvature of surfaces at the contact point or region. Anyway it could be convenient to make joint congruence independent from both contact point and curvature, for many reasons. First, the definition of the curvature require a parametrization of the surfaces. Anyway, discontinuous representation of the bones, as a mesh for example, are more common and easy to manage. Also, the contact may take place on multiple points, lines or surfaces, making though to employ such a definition. Finally, a measure independent form the bone to be in contact permits to characterize the entire space of joint configurations.

For the same reasons, Sirkett et. al [27] tried to use a geometrical measure of the contact area. They defined to be in contact those portions of surfaces that were distant to each other less than a given threshold. The problem of such a measure is that any area element under the threshold contributes in the same way. Anyway, the more two infinitesimal element are far from each other the more the two objects should be deformed before that these elements come in contact and start to contribute to the load redistribution. In other words, the contribution of each area

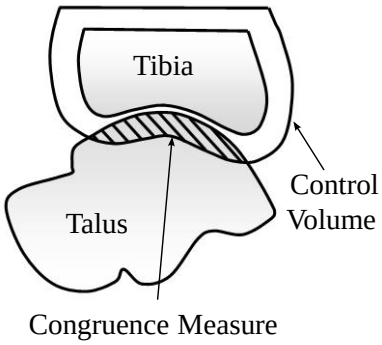

Figure 2.3: A 2D representation of the joint congruence measure.

element decreases while its distance rises. As a consequence it seems reasonable to weight each area element with its distance. A surface times a distance gives a volume and indeed a volume will be the measure we will employ to circumvent all the problems just presented. For this purpose we define a control volume comprised between the articular surface of a bone and an offset of the same surface. Then, in each configuration of the joint, we measure the congruence as the intersection of this volume with the second bone volume (Fig. 2.3). Clearly, the better the two surface mate, the bigger will be this intersection. Position leading to compenetration between the bones will be discarded, assigning to them a null value.

Chapter 3

Materials and metods

3.1 Ankle anatomy

The human ankle joint is formed by several anatomical parts. They can be divided into passive and active structures. Passive are called those elements which can exert forces only if externally stressed: articular surfaces, ligaments and other ligamentous structures belong to this category. On the contrary, active structures, such as the muscles, can intrinsically exert forces but, in general, they almost do not oppose external forces when inactive. For the aims of this dissertation we will focus only on the bones and the articular surfaces.

The ankle joint features three main bones: the tibia which forms the inside, or medial, portion of the ankle; the fibula which forms the lateral, or outside portion of the ankle; and the talus underneath (Fig. 3.1).

Figure 3.1: Anatomy of the ankle joint.

Furthermore, the bottom of the talus sits on the heelbone, called the calcaneus. This two foot bones are connected to make the subtalar joint, also known as the taluscalcaneal joint. The lateral malleolus of the fibula, the medial malleolus of the tibia and its distal inferior surface articulate with three facets of the talus. The relevant literature reports conflicting deductions regarding the number of degrees of freedom (dof) of the ankle joint and contradictory observations on geometry and pattern of contact of the articular surfaces [16, 28]. The most recent findings shows that the motion at the articulation between the inferior surface of the talus and the superior surface of the calcaneous, i.e. the subtalar joint, is considerable only when deviation forces are applied in the transverse and frontal planes but is very small in passive motion [15, 17]. In the latter condition, large spatial motion occurred solely at the tibiotalar joint, apparently guided by the passive structures alone. Contact occurs at the upper articulations, medial and lateral, of the talus with the tibial mortise, also between the lateral talus and the internal distal fibula.

3.2 Ankle joint coordinate systems

In order to follow the rigid relative motion among the bones in the ankle joint it is necessary to define some reference frames. Since the calcaneous is considered as rigidly joined with the talus (talus-calcaneal segment) and the fibula is considered as rigidly attached to the tibia (tibio-fibular segment), the passive motion of the ankle joint can be described by means of just two anatomical frames fixed on the tibio-fibular segment and talus-calcaneal segment respectively. It is convenient to define these frames anatomically; for this scope some anatomical landmarks were digitized.

The tibia-fibula anatomical reference system was defined as follows, according to a known convention [3]:

- origin: located at the midpoint between the tips of the lateral and medial malleoli;
- x-axis: the line perpendicular to the quasi-frontal plane defined by the tips of the malleoli and the head of the fibula, and pointing anteriorly;
- z-axis: the line connecting the tips of the malleoli, and pointing to the right hand side of the body;
- y-axis: orthogonal to the previous two, according to the right hand rule.

Likewise, the talus-calcaneus anatomical reference system was defined as follows:

- origin: located at the midpoint between the tips of the posterior ends of the lateral and medial ridges of the trochlea tali;
- y-axis: the line perpendicular to the quasi-transverse plane defined by these posterior tips and the head of the talus, and pointing proximally;

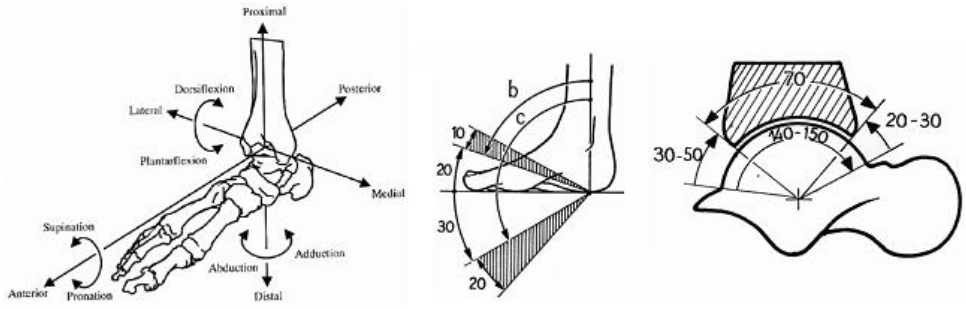

a) b)

Figure 3.2: Axes of rotation a) and range of motion b) for the ankle.

- x-axis: the line connecting the origin and the head of the talus, and pointing forward;
- z-axis: orthogonal to the previous two, and pointing to the right according to the right hand rule.

As known, for the definition of the relative position between two frames, six parameters are needed, three for translation and three for orientation. To define the latter, a sequence-independent joint coordinate system [12] was adopted. The three following axes were chosen: the y-axis of frame fixed to the tibia, the z-axis of that fixed to the talus, and a floating axis defined by the cross vector product of the formers. Three angles about these axes were defined respectively (Fig. 3.2.a): y-axis rotation, ankle internal$(+)$/external$(-)$rotation, z-axis rotation ankle dorsiflexion$(+)$/plantarflexion$(-)$, and floating axis of rotation, ankle pronation$(+)$/supination$(-)$. Internal and external rotation are also known as adduction and abduction rotation respectively. The range of the plantarflexion and dorsiflexion of the ankle joint is shown in Figure 3.2.b.

It is worth noticing that, to maintain the same clinical meaning for the rotations, when considering a left leg, the axes for the intra-extrarotation and for the prono-supination must be chosen with inverted direction.

3.3 Data acquisition

Passive motion of the talus with respect to the tibia was recorded for three specimen as a sequence of neutral equilibrium configurations during in vitro experimental sessions. Data were collected at the Movement Analysis Laboratory of the Istituti Ortopedici Rizzoli (IOR), which provided also the experimental facilities and the indispensable surgical and technical assistance. The data acquisition was performed by means of a surgical navigation system with cluster of active markers attached to the tibia and talus (Fig. 3.3). The anatomical geometry of the articular surfaces was digitalized as a grid o tridimensional coordinates recorded by means of a pointer.

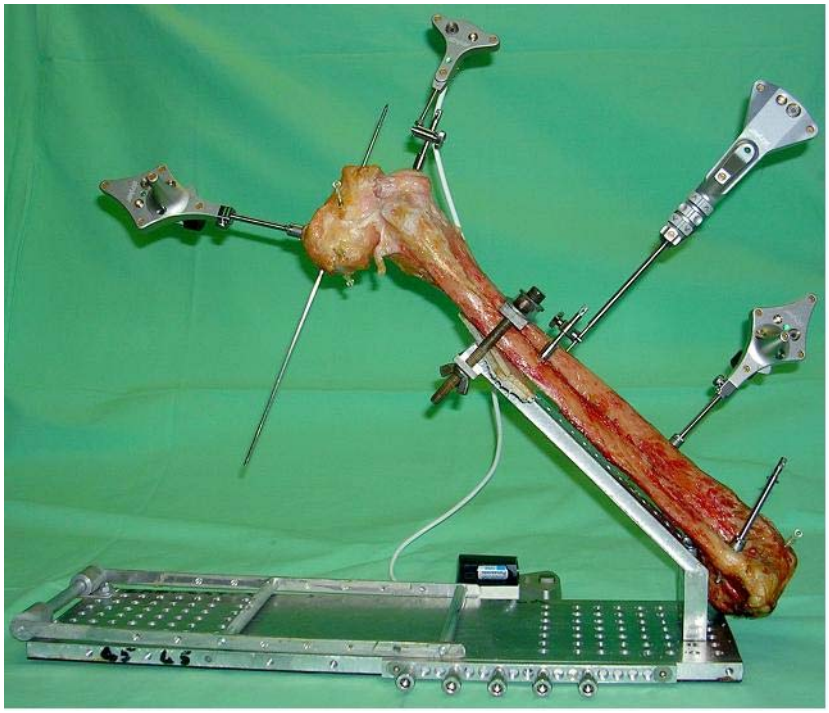

Figure 3.3: Experimental setup.

Each specimen, including the intact tibia, fibula, talus and calcaneous, was dissected at the Lisfranc joint line, freed of all skin, subcutaneous and muscle tissues, leaving joint capsule, interosseous membrane and ligaments intact. A careful inspection of the specimens confirmed that they were not affected by deformations or arthritis. The tibia was fixed to an oblique arm at a horizontal workbench, with the toes upwards, whereas the other bones were left free to move [15]. A pin drilled along the calcaneous longitudinal axis and protruding from the posterior surface came into contact with a rigid link, connected to the workbench by a revolute pair with axis parallel to the horizontal plane, which drove the pin to move with a five-DOF relative motion with respect to the link itself. An additional pin joined the talus to the calcaneous, forcing the subtalar joint to have no relative motion. Starting from a rest position in maximum plantarflexion, the ankle was driven to dorsiflexion by moving the rigid link up and down, until maximum dorsiflexion, thus producing flexion at the talus with respect to the tibia. Since the weight of the talus and the friction between the pin and the rigid link are negligible, the motion can be considered as in a virtually unloaded condition. An opto-electronic based motion tracking system (Stryker Navigation System) was used for recording the pose of the two trackers, fixed to tibia and talus according only to rigidity of the fixation and visibility of the trackers by the cameras. The camera system collected the pose of the two trackers and of the pointer in a definite workspace. The pose of the trackers was measured with respect to a Cartesian reference system fixed to the

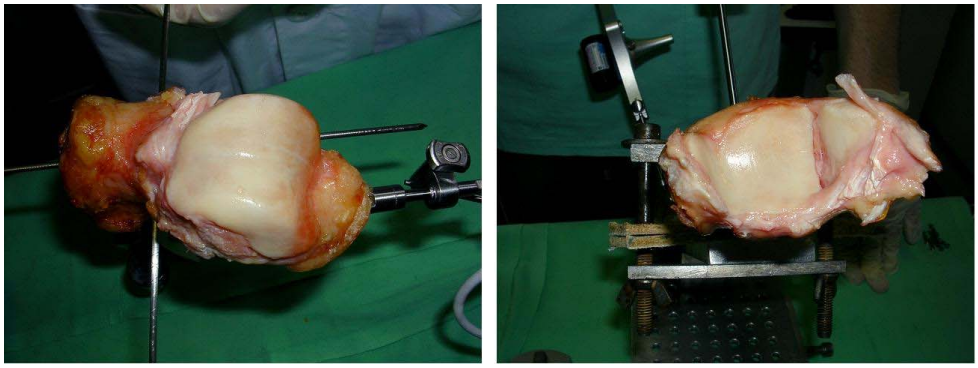

a) b)

Figure 3.4: The tibio-talar articular surfaces for a) the talus and b) the tibia.

camera system while the coordinates of points measured by the pointer are given in the reference system of the relevant tracker. For each leg preparation, multiple dorsi-plantar flexions were recorded. The specimens were further dissected and the geometry of the articular surfaces (Fig. 3.4) were digitized by means of the same pointer.

3.4 Bones modeling

Similarly to Marai et al. [19], in this work bones are modeled with a double representation, implicitly by means of a distance field and an explicitly with a triangular mesh. These two types of representation have complementary strength for different types of calculations. Explicit surfaces provide an accurate and relatively smooth representation of the bones. Distance fields (or maps), on the other hand, have important advantages for geometric computations such as fast distance calculation, collision detection, and inside-outside tests.

The algorithm for the generation and management of distance maps was kindly provided by Luca Tersi [29] as a C++ library. Briefly, a distance field is an octree-based representation of an object [14, 34]. In this representation, the volume outside and inside the surface of the object is non-uniformly discretized by assigning to each point of the discretization the corresponding signed distance from the surface of the model: positive if outside, negative if inside the object. The distance is computed as the minimum distance between the discretization point and the surface of the object to be modeled, here a bone. The distance map structure is an octree built with an iterative procedure, subdividing a cube (also called octant) iteratively in other 8 half-side octants when it contains at least one point bone surface. The vertices of the octants are the volume discretization points. The distance of a generic point from the surface is then computed with a tri-linear interpolation of the distances of the 8 vertices of the smallest octant containing the point. The octant side dimension gets smaller closer to the surface, thus the interpolation error

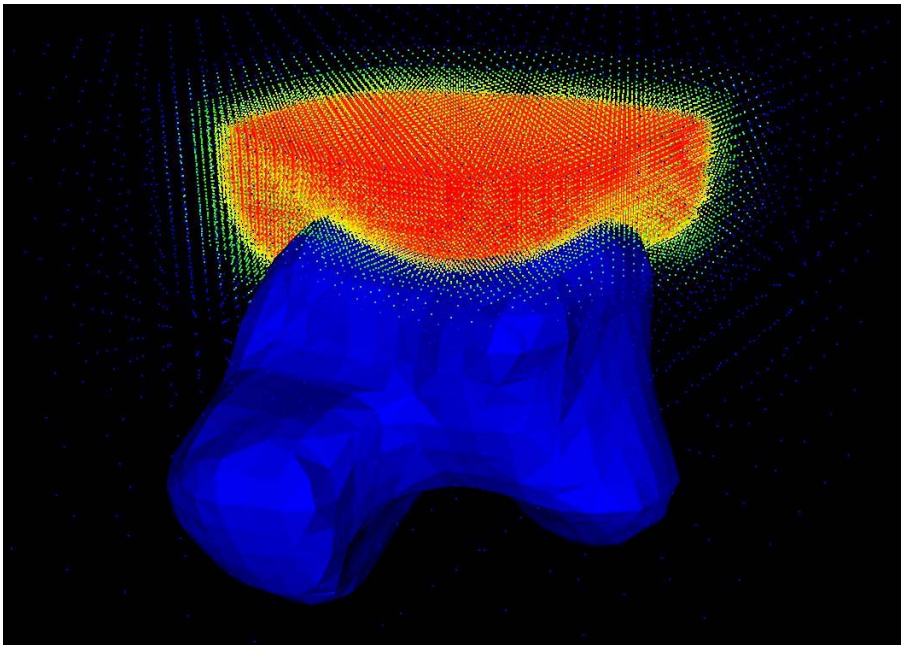

Figure 3.5: Distance map and mesh representation for the tibia and the talus, respectively.

becomes negligible.

Triangular mesh models for the bones were found in the VAKHUM database (www.ulb.ac.be/project/vakhum). Those models have been manually adapted to fit the experimental data for the articular surfaces by both scaling them and remodeling their mesh so to include the points obtained by the digitalization of the bone articular surfaces.

Since in this dissertation the relative motion take place between the tibia and the talus, only this two bones are modeled.

Figure 3.5 shows the mesh for the talus surface, in blue, and the distance field representing the tibia. The points are colored according to their distance from the tibia surface. As it possible to see, the cloud of points becomes thicker in the neighborhood of the bone.

3.5 Numerical measure of the joint congruence

As already introduced in the Section 2.3, we measure the joint congruence as the intersection of the volume of talus with a control volume, obtained by offsetting of a prescribed threshold the articular surfaces of the tibia (we report here Fig. 2.3 as Fig 3.6.a for sake of convenience).

The evaluation of this volume may be directly obtained as the result of a Boolean difference. This operation is for example possible using the GNU Tri-

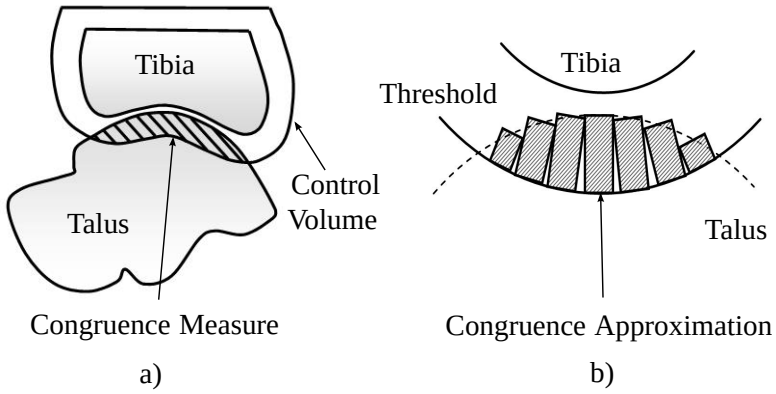

Figure 3.6: A 2D representation of a) the joint congruence measure and b) its approximation.

angulated Surface (GTS) C++ library. Although precise, this measure is computationally very expensive. It is thus more convinient to resort to an alternative evaluation of the intersection volume, approximating it as the sum of small discrete contributions. Essentially, by means of the distance maps, all the triangles of the talus mesh laying inside the control volume are detected. The area of each element is then multiplied by its distance from the offset surface and add to the joint congruence measure (Fig. 3.6.b). The triangle distance is defined as the mean of its vertex distances from the same surface. All the distances are evaluated by means of the distance map representing the tibia. This procedure has proved to be faster than Boolean computations among the same volumes, without affecting the results. A collision detection is also possible by means of the distance map. It is sufficient to check if any triangle of the talus mesh has a distance smaller or equal to zero. In this case, the measure of the joint congruence is set to zero.

3.6 Trajectory generation

As known, the relative position between two bones is described by six spatial coordinate, three for the orientation and three for the translation. Together they identify the bones relative pose. If the considered joint has n dof, its kinematics can be parameterized by means of n coordinates. This means that, prescribing n coordinates, the remaining $6-n$ are determined by the constraint that made the joint a n dof one. During its passive motion, the tibio-talar joint may be considered as a single dof joint [15] and can thus be parameterized with the dorsi-plantar flexion angle. Once that a value for the flexion is given, all the other pose coordinates are implicitly defined by the constraint acting during passive motion. To explicit their values, we hypothesize that passive motion satisfy the Wollf's Law and thus we impose the congruence maximization. In other words, keeping fixed the flexion angle, the other pose coordinates will be found as those that maximize the joint

congruence.

The trajectory of the tibio-talar passive motion is obtained as the envelop of successive maximum congruence poses by subsequent optimization with a customized genetic algorithm (programmed on the base of GAlib C++ library). Starting from an initial guess, usually taken from experimental measures, a grid of poses is built representing a neighborhood around it. This contains all the possible combinations of coordinates variation of a small amount δ, keeping the flexion fixed. Further configurations are added to this neighborhood exploiting the genetic algorithm techniques: mating and mutation. A (objective) function of the joint configuration is then evaluated in each of these pose, returning a measure of the joint congruence. Around the configuration with the maximum congruence a new neighborhood is built and the analysis repeated. This procedure continues until a (local) maximum is reached. The best pose is added to the trajectory and then used as initial guess for the next optimization, after its flexion angle has been incremented. This procedure is repeated on the whole flexion range, resulting in a spatial trajectory. To increase the reliability of the algorithm, more than one neighborhood was usually taken at each step, obtained with increasing value of δ. The conceptual flow of the validation procedure for this algorithm is depicted in Figure 3.7.

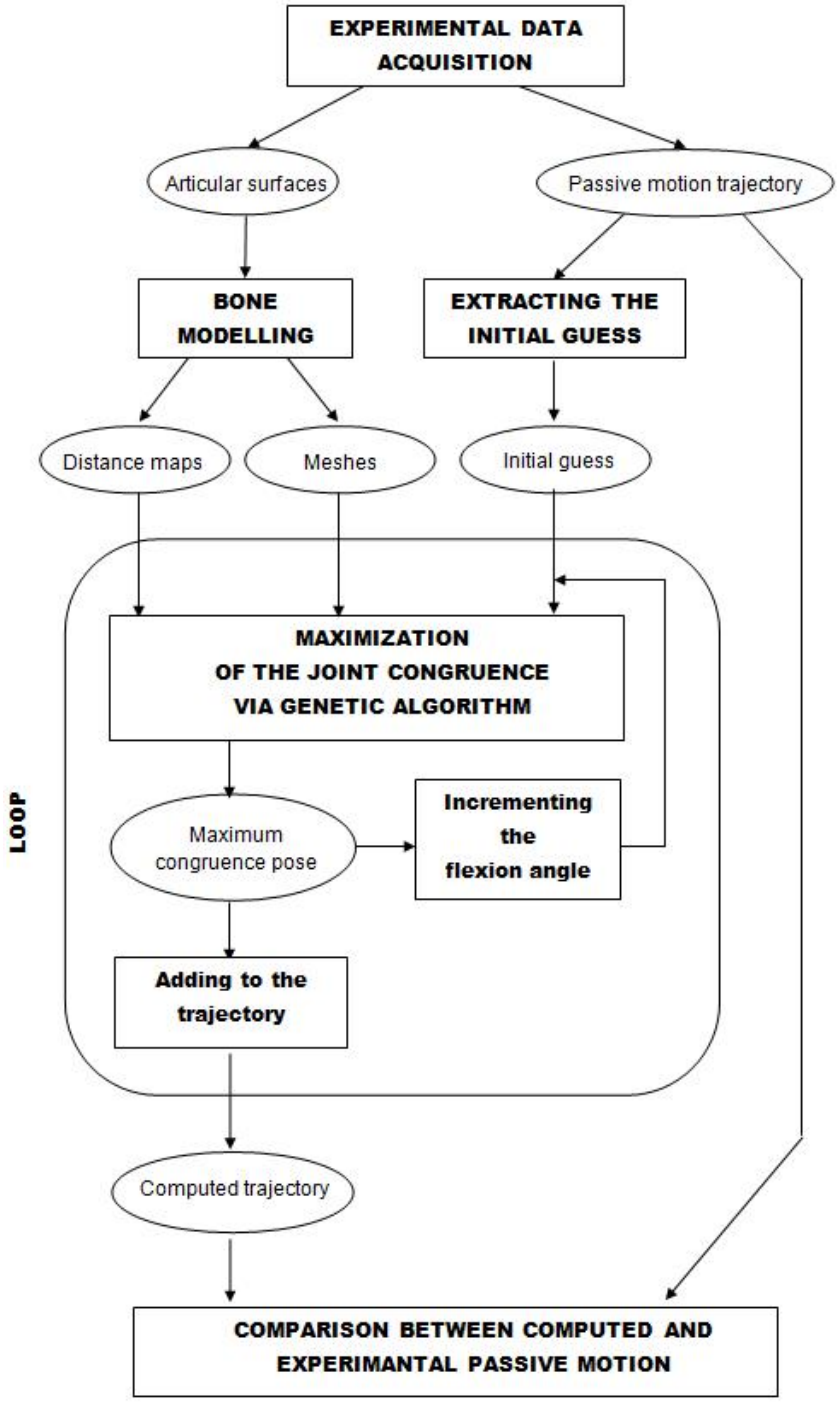

Figure 3.7: A pipeline of the algorithm for the trajectory generation and validation.

Chapter 4

Results and discussion

4.1 Results

Figure 4.1 shows the maximum congruence trajectory computed for the three specimens, together with the anatomical passive motion poses measured experimentally. The first plot of each Figure shows the progression of the prono-supination and intra-extra rotation angles while the second shows the progression of the x, y and z displacements, all plotted versus the dorsi-plantar flexion angle. Dotted lines represent the path obtained as mean of experimental trajectories, while continuous lines shows the computed ones. To statistically characterize the model behavior we turn to the evaluation of mean absolute errors (MAE) for each component of the passive motion. It is defined as

$$MAE = \sum_{i=1}^{p} (\|x_i - \bar{x_i}\|) \tag{4.1}$$

where p is the number configurations composing the parametrized trajectory, x_i is the computed value of the generic component and $\bar{x_i}$ it is the measured one, both evaluated at the same ith value of the flexion angle.

The MAEs for prono-supination, intra-extra rotation and the displacements for the three specimen are summarized in table 4.1.

Results for the first and the second specimens show a bad approximation of the experimental data. Let us hypothesize that this behavior is caused only by an error in the reconstruction of the frames we use for express the trajectories, the relative motion still being the same. If this is the case, computed and experimental curves differ just for a rototranslation, describing in fact the same path within a constant rigid error. To test this idea, we may compute the transformation that brings two poses of computed and experimental trajectories to coincide for a prescribed flexion angle. Let us assume that this transformation represent the constant relative error between the two. Thus applying the transformation to the whole computed one we should be able to achieve a better match. The results after this operation are shown in Fig 4.2, while Tab 4.2 report the new mean absolute errors. Both a

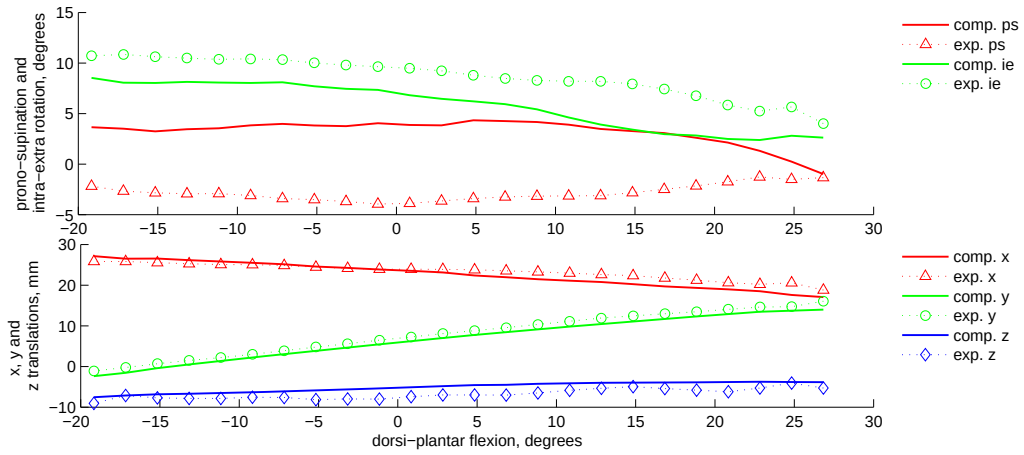

a)

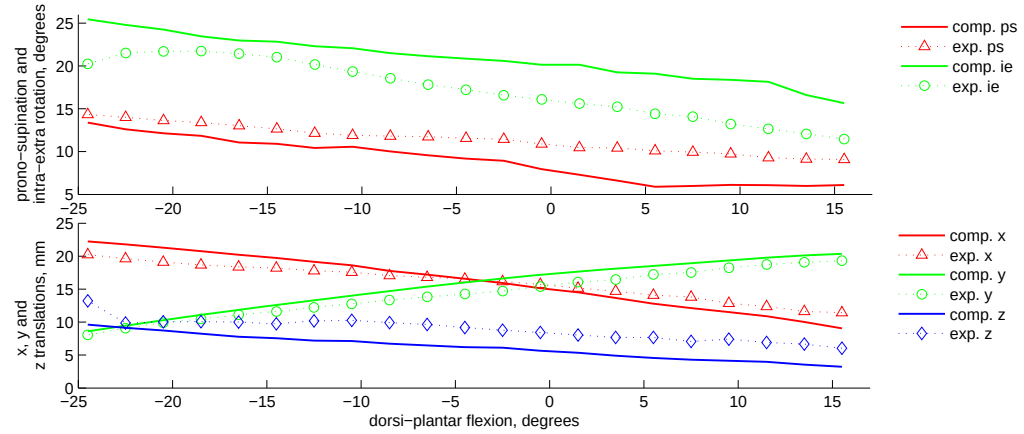

b)

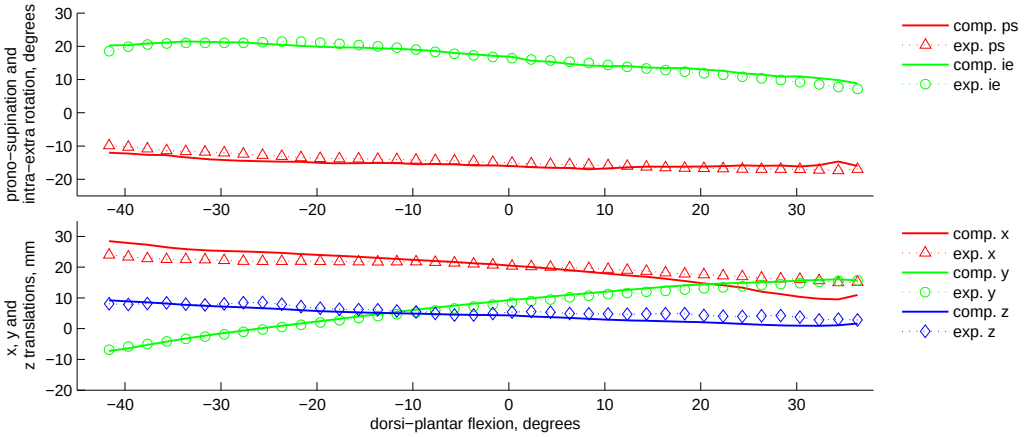

c)

Figure 4.1: Computed (comp) and experimental (exp) prono-supination (ps), intra-extra rotation (ie) and x, y, and z displacements versus dorsi-plantar flexion for the a) first, b) second and c) third specimen, respectively.

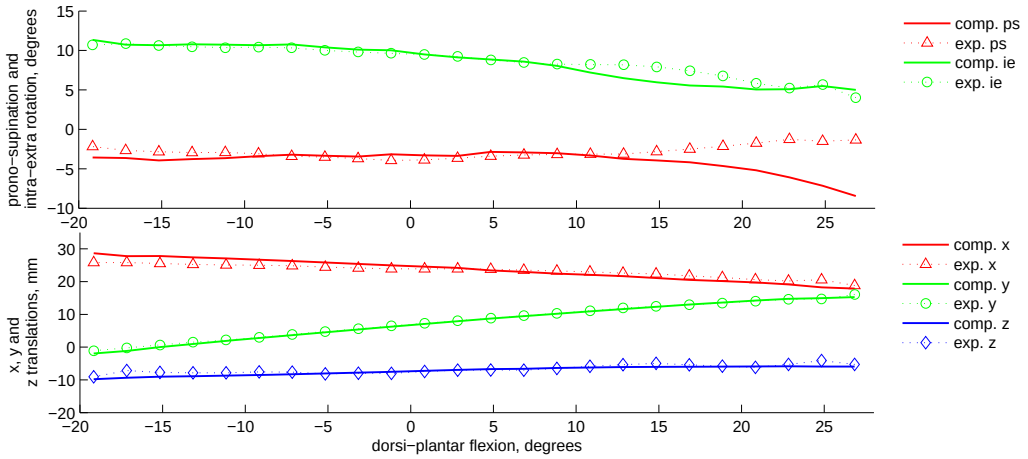

a)

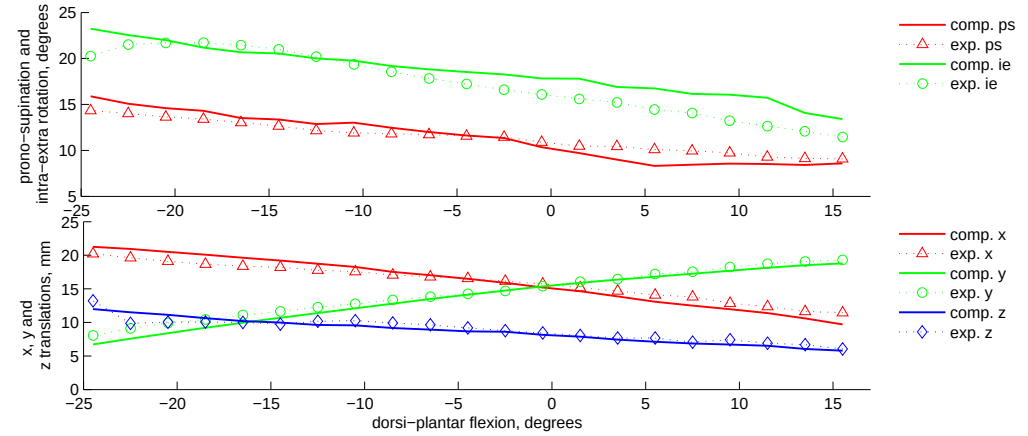

b)

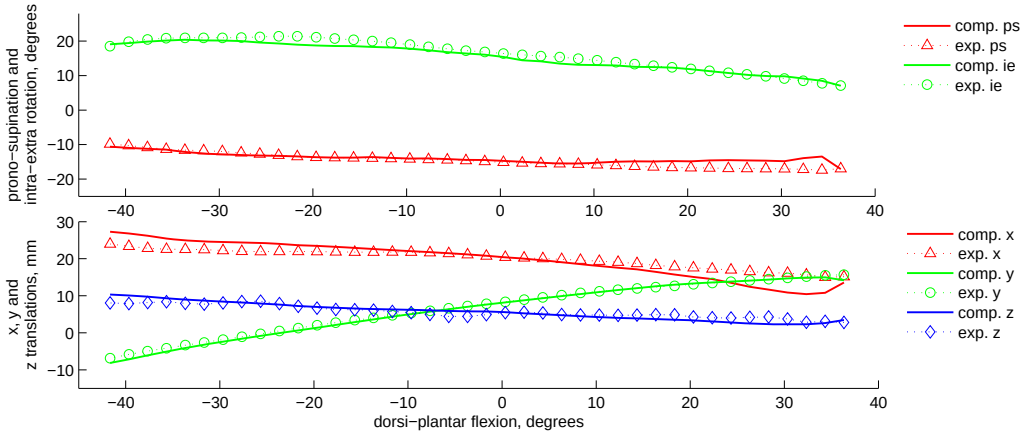

c)

Figure 4.2: Computed (comp) and experimental (exp) prono-supination (ps), intra-xtra rotation (ie) and x, y, and z displacements versus dorsi-plantar flexion for the a) first, b) second and c) third specimen after correction with a constant rigid rototranslation.

Table 4.1: MAE for the five coupled components of passive motion.

	Prono-supination (degrees)	**Intra-extra rotation (degrees)**	**X (mm)**	**Y (mm)**	**Z (mm)**
1^{st} **leg**	6.0214	2.8523	1.2273	1.1411	1.6530
2^{st} **leg**	2.4804	3.6166	1.3157	1.1702	2.6810
3^{st} **leg**	1.2538	0.7505	2.4933	0.7346	1.3880

Table 4.2: MAE for the five coupled components of passive motion after correction with a constant rigid rototranslation.

	Prono-supination (degrees)	**Intra-extra rotation (degrees)**	**X (mm)**	**Y (mm)**	**Z (mm)**
1^{st} **leg**	1.4859	0.5716	1.3023	0.2996	0.6529
2^{st} **leg**	0.8452	1.4798	0.9015	0.6371	0.5616
3^{st} **leg**	0.8931	0.9948	1.9779	0.4388	0.8453

qualitative inspection of the plot and a numerical comparison of the errors show a great improvement in the matching, particularly evident for the rotations.

The computed trajectories was generated along a plantar flexion motion. Looking at the plots it is possible to notice that, at the beginning of the plantar flexion, so on the right side of the plot, the curves seem affected by an error that is gradually corrected. This is particularly evident for the prono-supination in first specimen and, to a smaller degree, for the intra-extra rotation of the second one. This behavior is in agreement with the hypothesis of a constant error, since the initial guess employed as a start for the trajectory computation comes from the experimental measures. To further verify this hypothesis, new trajectories has been computed, taking as initial guess the beginning of experimental plantar-flexion after applying T^{-1}. The new curves and mean absolute errors are shown in Fig. 4.3 and Tab. 4.3, respectively.

The previous reasoning seems to validate the idea that the model predictions differ from experimental data only by a constant error, a rigid rototranslation, this being ascribable to some misalignment between the bones model and the recorded data. It is anyway still not possible to know if the constant error belong to the computed trajectories or the measured ones. A visual evaluation of the motion obtained into the two case shows anyway a better behavior for the computed motion, by this meaning that the joint present a much uniform coupling. It is thus possible to think that the error was made while registering the markers used for the anatomical frames definition.

Table 4.3: MAE for the five coupled components of passive motion after correction of the initial guess

	Prono-supination (degrees)	**Intra-extra rotation (degrees)**	**X (mm)**	**Y (mm)**	**Z (mm)**
1^{st} **leg**	0.6079	0.7404	1.7551	0.3071	0.5906
2^{st} **leg**	0.5435	0.9048	0.8133	0.6081	0.5129

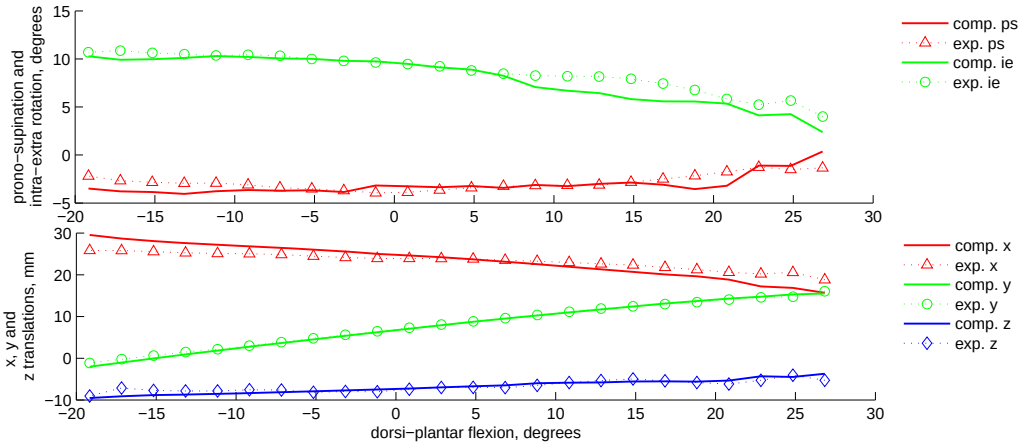

a)

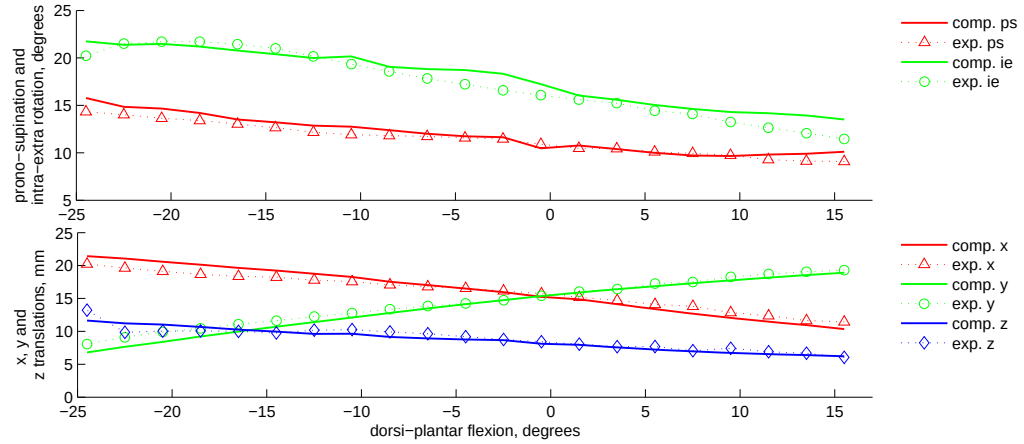

b)

Figure 4.3: Computed (comp) and experimental (exp) prono-supination (ps), intra-xtra rotation (ie) and x, y, and z displacements versus dorsi-plantar flexion for the a) first and b) second specimen after correction of the initial guess.

Table 4.4: Mean standard deviation (MSD) and absolute errors (MAE) for multiple launches of the algorithm.

	Prono-supination	**Intra-extra rotation**	**X**	**Y**	**Z**
MSD	0.5136	0.8586	0.1990	0.1168	0.2786
MAE	1.8634	0.7228	2.6027	0.6785	1.6384

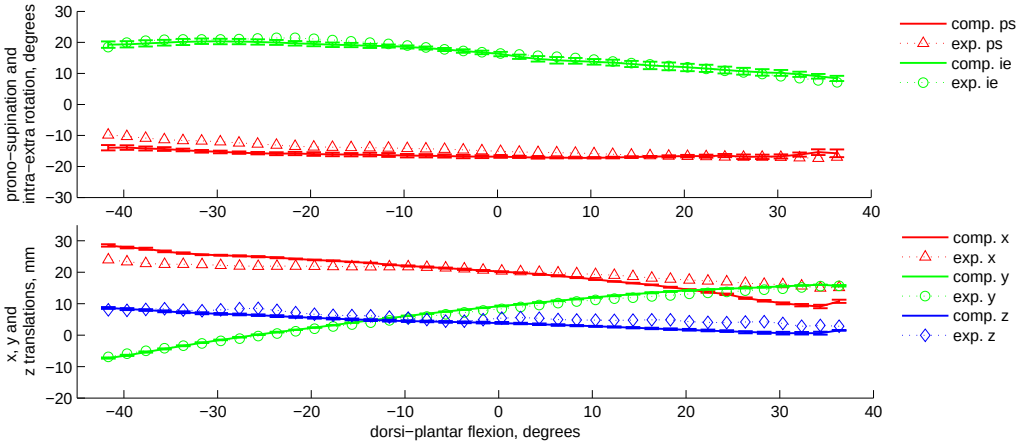

Figure 4.4: Computed (comp) and experimental (exp) prono-supination (ps), intra-extra rotation (ie) and x, y, and z displacements versus dorsi-plantar flexion for the third specimen as mean of multiple launches with the same algorithm parameters.

4.2 Sensitivity analysis

An important aspect for the validation of the model proposed in this dissertation is the analysis of its sensitivity to the parameters that define it and that may thus affect its outcome.

The genetic algorithm exploit for the optimization of the joint congruence introduce a random component in the computation, due to the method employ for give the birth to new generation. This can obviously influence its repeatability. Another factor that potentially may affect the algorithm behavior is the threshold used to define the control volume. It determines indeed how much of the talus surface is considered for the congruence computation. Also worth to be studied is the effect of the density of the distance map, i.e. the refinement of the implicit representation of the tibia. Last but not least, the variations introduced by the choice of the initial guess have a great relevance, as for every optimization algorithm.

The third specimen was chosen to perform the sensitivity analysis, being the one that shows less difference between computed and measured passive motion, even without corrections.

A preliminary analysis has shown that, despite the random component, the

Table 4.5: MSD and MAE for variations of side of the smaller cube into the distance map in the range from 0.5 to 2.5 mm.

	Prono-supination	**Intra-extra rotation**	**X**	**Y**	**Z**
MSD	0.4963	0.6646	0.1508	0.0913	0.2322
MAE	1.9345	1.0278	2.6060	0.6343	1.7064

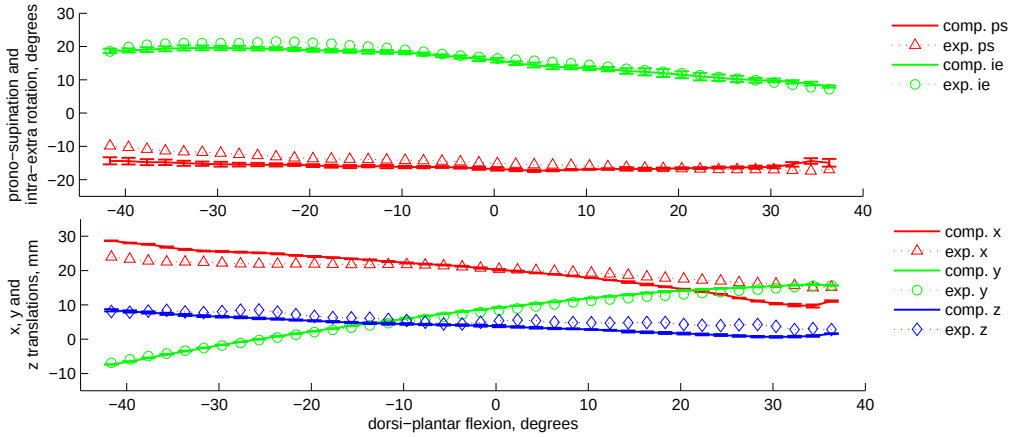

Figure 4.5: Computed (comp) and experimental (exp) prono-supination (ps), intra-extra rotation (ie) and x, y, and z displacements versus dorsi-plantar flexion for the third specimen as mean of computations with different value for side of the smaller cube into the distance map, varying between 0.5 and 2.5 mm.

algorithm is highly repeatable. In fig 4.4 are represented the mean experimental and computed trajectory, after multiple launches. For the latter also the standard deviation is represented. For each pose coordinate, the MAE between the mean of the computed trajectories and the mean experimental one is reported in the Tab. 4.4, together with the mean standard deviation (MSD). This is defined as

$$MSD = \sum_{i=1}^{p} \sigma_i \tag{4.2}$$

where p is the number configurations composing the parametrized trajectoryand σ_i is the standard deviation between mean computed and mean measured trajectory evaluated at the same ith value of the flexion angle.

As shows by the mean standard deviation, multiple launches of the algorithm with the same parameters produced well grouped trajectories. Also, the MAE is very close to that of the single trajectory (see Tab. 4.1).

To study the influence of the distance map refinement, the value of its smaller cube side was varied from 0.5 to 2.5 mm, showing no significant variation among the computed trajectories(see Fig. 4.5 and Tab. 4.5).

Table 4.6: MSD and MAE for values of the control volume threshold in the range from 2 to 11 and from 4.5 to 11 mm.

	Prono-supination	Intra-extra rotation	X	Y	Z
		2÷11			
MSD	3.6239	2.5701	1.9867	0.5820	2.5009
MAE	3.3672	3.8489	1.2548	1.0199	1.7506
		4.5÷11			
MSD	0.3773	0.6005	0.1928	0.0989	0.1970
MAE	1.7858	0.5545	2.5709	0.7113	1.5445

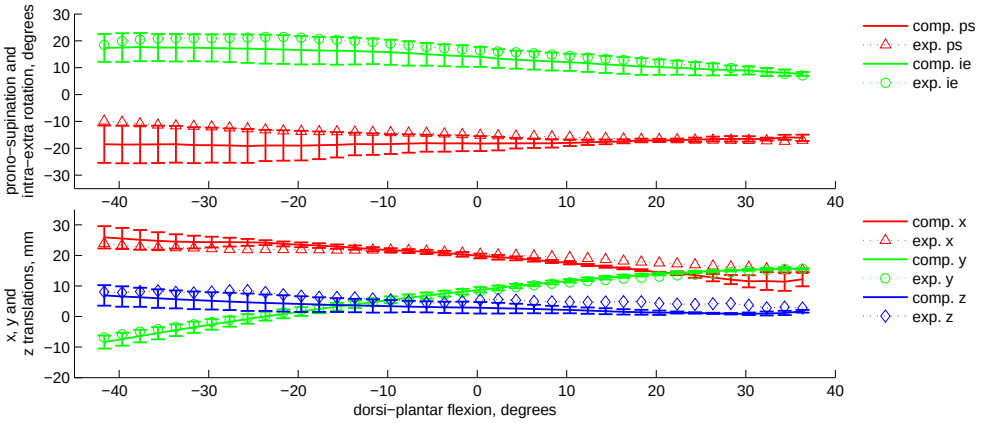

a)

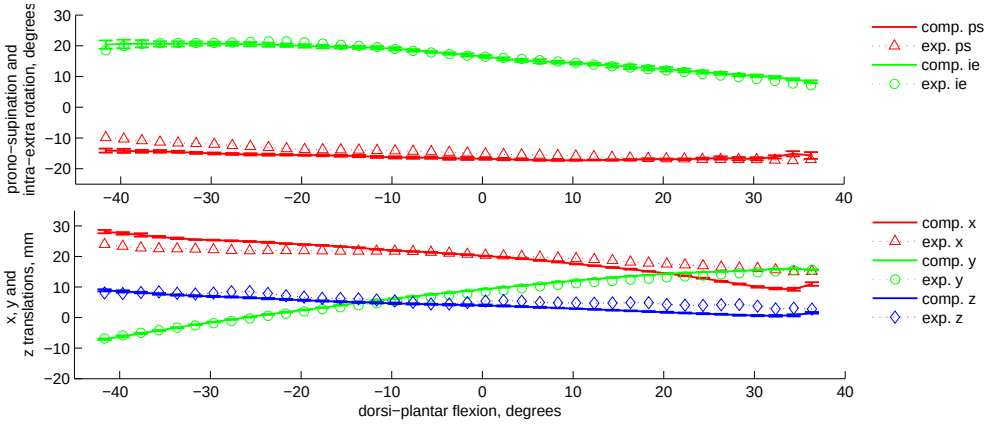

b)

Figure 4.6: Computed (comp) and experimental (exp) prono-supination (ps), intra-extra rotation (ie) and x, y, and z displacements versus dorsi-plantar flexion for the third specimen as mean of computations with different values for the control volume threshold, varying between a) 4.5 and 11 and b) 4.5 and 11 mm.

Table 4.7: MSD and MAE for variations of the original initial guess components but flexion of a same amount in the range from -5 to $+4$ mm.

	Prono-supination	**Intra-extra rotation**	**X**	**Y**	**Z**
MSD	0.4963	0.6646	0.1508	0.0913	0.2322
MAE	1.9345	1.0278	2.6060	0.6343	1.7064

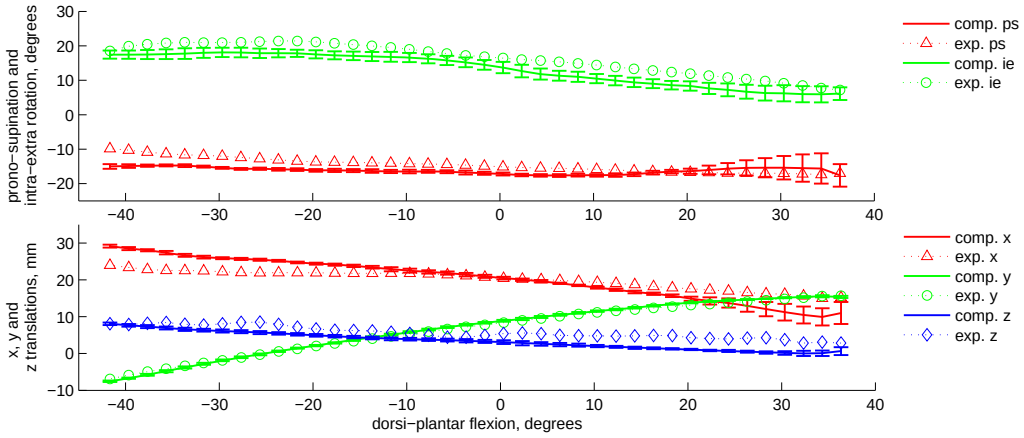

Figure 4.7: Computed (comp) and experimental (exp) prono-supination (ps), intra-extra rotation (ie) and x, y, and z displacements versus dorsi-plantar flexion for the third specimen as mean of computations with different initial guess, obtained by varying the original of a same amount in all the coordinates but the flexion angle, in a range between -5 and $+4$

The threshold defining the control volume has been manually chosen. Token an anatomical pose, its value was incremented, thus increasing the talus surface intersecting the control volume, as long as the new area was still belonging to the articular surface and not to other part of the bone. This lead to an optimum value of 7. The analysis of the algorithm sensitivity to the control volume threshold has shown that the congruence measure fails to drive the simulation for a value of 2mm, it produces noticeable discrepancy from the experimental path for a threshold of 3 mm but the agreement lays in the repeatability in the range from 4.5 up to 11 mm. Figure 4.6.a shows the standard deviation and mean computed trajectory in the range from 2 to 11, while Fig. 4.6.b deos the same for the range from 4.5 to 11. Table 4.6 reports the MSD and the MAE for the two cases.

Finally, to take into account the effect of different initial guesses, the original one has beex varied by incrementing of a same amount all the coordinates but the flexion angle, in a range between -5 and $+4$. The results are shown in Fig. 4.7 and in Tab. 4.7.

A visual analysis of the single trajectories shown that in the range $-5 \div +1$ the

trajectory variations are still ascribable to the algorithm repeatability, while in the range $+1 \div +4$ they become more sensible to the initial guess choice, especially for the intra-extra rotation, which in some point differs from experimental data up to 10 degrees. The choice of the initial guess plays surly a fundamental role in determining the behavior of the algorithm, and their relation is highly non linear. Anyway, is worth noticing a trend visible in Fig. 4.7: after a first assessment, the trajectories still tend to converge to the experimental motion, as the progressive reduction of the standard deviation shows.

4.3 Discussion

The reduced number of specimen tested together with the small number of total simulations performed allow exclusively preliminary considerations. Nevertheless, the results show a general good agreement between computation and experimental data. In general, errors seem to affect more the rotations than translations, the algorithm being also more repeatable for the latter than for the formers. This behavior appears reasonable considering the non linearity connected with the rotations. It is anyway interesting to notice that the mean absolute error for the x displacement has usually an high value. Unlike the other components, it also does not show big improvement after the correction of the rigid error. This may be caused by the smaller rigidity of the ankle into the anterior direction, possibly indicate an error in the experimental measure connected to the weight of the talo-calcaneous segment and the instrumentation fixed to it.

A preliminary sensitivity analysis indicate the model to by repeatable in spite of the random component introduced by the genetic component of the algorithm. It is also little sensitive to the variation of the threshold defining the control volume employed for the congruence measure, especially over the value of 4.5 mm, and insensitive to the distance map refinement. The most important factor determining the algorithm outcome appear to be the initial guess. Still, the algorithm proved to be robust to its variation, tending to correct the initial error during the progression of the computation.

Chapter 5

Limitations of the model

The principles employed in the generation of the kinematic model for the ankle passive motion are very general. It is thus quite straightforward imagining to extend the same concept to other joints. Anyway, some observation are worth to be done

The model developed in this model is not suitable for joint with full congruence on the whole range of motion, such as the hip or the shoulder. The almost ball-socket coupling in these joints preserve the congruence near to a constant value, making each position energetically equivalent.

More in general, in multi-dof joints, the research of the maximum congruence pose may result in an indeterminate problem, possible existing n dimensional isoenergetic surfaces. This is potentially the case of the wrist. For this reason an interesting challenge could be the research and definition of a one dof minimum energy path for each new joint to be investigated.

A difficult task is also the extension of the model when we want to consider multiple bones in the joint. Indeed, optimization methods employing derivatives, although computationally faster, had proved to produce poor result when compared to the slower genetic approach. This may be due to the high non linearity of the joint congruence. The simple evaluation of its increment respect to the variation of the single pose coordinates is not sufficient, and all the possible combination of the coordinates variations have to be considered. Unfortunately, it is easy to show that the number of this combination N_d is equal to

$$N_d = 3^{\sum_{i=1}^{b-1}(6-dof_i)} \tag{5.1}$$

where b is the total number of bones in the considered joint and dof_i the degrees of freedom of the i^{th} of them. For the ankle as modeled in this dissertation, it will lead to $3^5 = 243$ possible direction of increment to be evaluated. For a joint as the wrist, considered as a two dof and composed by eight bones, this lead to 3^{40}. The geometrical growth with the number of bones simply make computationally impossible to directly extend the genetic approach developed here.

Also, it is possible to neglect the constraint imposed by the ligaments between

contacting bones because the minimum energy principle allow us to extract the information on the relative motion from the shape of the articular surface. Anyway, once that the two bone connected by ligaments are no longer directly in contact, this may be no more true.

Finally it is worth noting that the algorithm presents a non isotropic behavior. Predictions obtained for the dorsi-flexion differ from those for the plantar-flexion and are in general less precise and stable. This can be due to the non symmetry into the talus articular surface, which at the beginning of the dorsi-flexion offer to the tibia a much smaller area, thus less suitable for the generation of motion guidance. This aspect surly deserves further studies.

Chapter 6

Conclusions

The presented work aimed to develop and test a kinematic model exploiting the Wolff's Law as a minimum energy principle.

Due to the small number of specimen studied, this has to be considered as a preliminary analysis. Anyway, the comparison between experimental and computed trajectories seems to validate the model for the tibio-talar joint on a range of more than 70 degrees of plantar flexion.

If further confirmed, this will indirectly prove both that the passive motion is a minimum energy path, thus provides a theoretical representation of it, and that the articular surfaces are shaped in agreement with the Wolff's Law for a maximization of the joint congruence.

In is important to underline the predictive nature of this model. Unlike most of other models in the literature, this does not rely on a measure of the trajectory it try to match. Also, unless very general this approach make possible to generate subject-specific models, requiring relatively simple anatomical measures. Finally, the sensitivity analysis shows the algorithm to be repeatable and robust.

Possible application of such a model may be found in pre-surgical planning, in the study of the degeneration of articular surfaces and in the prosthesis design.

Future works will aim to further validate this model on the ankle with more experimental analysis and to test its applicability on other joints, such the knee and the wrist.

Bibliography

[1] L. Blankevoort and R. Huiskes. Validation of a three-dimensional model of the knee. *Journal of Biomechanics*, 29(7):955 – 961, 1996.

[2] L. Blankevoort, J. H. Kuiper, R. Huiskes, and H. Grootenboert. Articular contact in a three-dimensional model of the knee. *Journal of Biomechanics*, 24(11):1019 – 1031, 1991.

[3] A. Cappozzo, F. Catani, U.D. Croce, and A. Leardini. Position and orientation in space of bones during movement: anatomical frame definition and determination. *Clinical Biomechanics*, 10(4):171–178, 1995.

[4] Jan-Hung Chen, Chao Liu, Lidan You, and Craig A. Simmons. Boning upon wolffs law: Mechanical regulation of the cells that make and maintain bone. *Journal of Biomechanics*, 43:108–118, 2010.

[5] K. D. Connolly, J. L. Ronsky, L. M. Westover, J. C. Kupper, and R. Frayne. Analysis techniques for congruence of the patellofemoral joint. *Journal of Biomechanical Engineering*, 131(12):1–7, 2009.

[6] R. Di Gregorio, V. Parenti-Castelli, J.J. O'Connor, and A. Leardini. Mathematical models of passive motion at the human ankle joint by equivalent spatial parallel mechanisms. *Medical and Biological Engineering and Computing*, 45(3):305 – 313, 2007.

[7] Raffaele Di Gregorio and Vincenzo Parenti-Castelli. A spatial mechanism with higher pairs for modelling the human knee joint. *Journal of Biomechanical Engineering*, 125(2):232 – 237, 2003.

[8] Ahmet Erdemir, Scott McLean, Walter Herzog, and Antonie J. van den Bogert. Model-based estimation of muscle forces exerted during movements. *Clinical Biomechanics*, 22(2):131 – 154, 2007.

[9] R. Franci and V. Parenti-Castelli. A one-degree-of-freedom spherical wrist for the modelling of passive motion of the human ankle joint. In A. Kecskemethy, editor, *Proceedings of IAK 2008, Conference on Interdisciplinary Applications of Kinematics*, pages 1–13, Lima, Peru, January 2008.

[10] Riccardo Franci, Nicola Sancisi, and Vincenzo Parenti Castelli. A three-step procedure for the modelling of human diarthrodial joints. In *Proceedings of the RAAD 2008, 17th International Workshop on Robotics in Alpe-Adria-Danube Region*, pages 1–10, Ancona, Italy, September 2008.

[11] Harold M. Frost. A 2003 update of bone physiology and wolffs law for clinicians. *Angle Orthodontist*, 74:3–15, 2004.

[12] E. S. Grood and W. J. Suntay. A joint coordinate systenf for the clinical description of three-dimensional motions: Application to the knee. *Journal of Biom.echilnlcal Engineering*, 135:136–144, May 1983.

[13] Mohamed Samir Hefzy and T.Derek V. Cooke. Review of knee models: 1996 update. *Applied Mechanics Reviews*, 49(10 pt 2):S187 – S193, 1996. Knee models;Patello femoral joints;Tibio femoral joints;.

[14] S. Lavallee and R. Szeliski. Recovering the position and orientation of free-form objects from image contours using 3d distance maps. *IEEE Transactions on Pattern Analysis and Machine Intelligence*, 17(4):378 – 90, 1995.

[15] A. Leardini, J.J. O'Connor, F. Catani, and S. Giannini. Kinematics of the human ankle complex in passive flexion; a single degree of freedom system. *Journal of Biomechanics*, 32(2):111 – 18, 1999.

[16] A. Leardini, J.J. O'Connor, F. Catani, and S. Giannini. The role of the passive structures in the mobility and stability of the human ankle joint: a literature review. *Foot Ankle Int*, 24(7):602–615, 2000.

[17] Alberto Leardini, Rita Stagni, and John J O'Connor. Mobility of the subtalar joint in the intact ankle complex. *Journal of Biomechanics*, 34(6):805 – 809, 2001.

[18] G.E. Marai. *Data-Driven Predictive Modeling of Diarthrodial Joints*. PhD thesis, Brown University., 2007.

[19] G.E. Marai, D.H. Laidlaw, C. Demiralp, S. Andrews, C.M. Grimm, and J.J. Crisco. Estimating joint contact areas and ligament lengths from bone kinematics and surfaces. *IEEE Transactions on Biomedical Engineering*, 51(5):790 – 9, 2004.

[20] M.G. Pandy, K. Sasaki, and S. Ki. A three-dimensional musculoskeletal model of the human knee joint. part 1: theoretical construction. *Computer Methods in Biomechanics and Biomedical Engineering*, 1:87–108, 1997.

[21] Vincenzo Parenti-Castelli and Raffaele Di Gregorio. *Parallel mechanisms applied to the human knee passive motion simulation*, pages 333–344. Kluwer Academic Publishers, Pirano-Portoroz, Slovenia, June 2000.

[22] E. Pena, B. Calvo, M.A. Martinez, and M. Doblare. A three-dimensional finite element analysis of the combined behavior of ligaments and menisci in the healthy human knee joint. *Journal of Biomechanics*, 39(9):1686 – 1701, 2006.

[23] Nicola Sancisi and Vincenzo Parenti-Castelli. A 1-dof parallel spherical wrist for the modelling of the knee passive motion. In *Proceedings of IFToMM 2007, 20th World Congress in Mechanism and Machine Science*, pages 1 1–6, Paper no. A94, Besançon, France, June 2007.

[24] Nicola Sancisi and Vincenzo Parenti-Castelli. A sequential approach for modelling knee joint stiffness. In *Proceedings of RoManSy 2008, 17th CISM-IFToMM Symposium on Robot Design, Dynamics, and Control*, pages 1–8, Tokyo, Japan, July 2008.

[25] K.B. Shelburne and M.G. Pandy. A dynamic model of the knee and lower limb for simulating rising movements. *Computer Methods in Biomechanics and Biomedical Engineering*, 5(2):149–159, 2002.

[26] William H. Simon, Steven Friedensberg, and Steven Richardson. Joint congruence: a correlation of joint congruence and thikness of articular cartilage in dogs. *Journal of Bone and Joint Surgery*, 55:1614–1620, 1973.

[27] D.M. Sirkett, G. Mullineux, G.E.B. Giddins, and A.W. Miles. A kinematic model of the wrist based on maximization of joint contact area. *Proceedings of the Institution of Mechanical Engineers, Part H: Journal of Engineering in Medicine*, 218(5):349 – 359, 2004.

[28] R. Stagni, A. Leardini, , J. J. OConnor, and S. Giannini. Role of passive structures in the mobility and stability of the human subtalar joint: a literature review. *Foot Ankle Int*, 24(5):402–409, 2003.

[29] Luca Tersi, Silvia Fantozzi, and Rita Stagni. 3d elbow kinematics with monoplanar fluoroscopy: in silico evaluation. *EURASIP Journal on Advances in Signal Processing*, pages 1–10, 2010.

[30] D.R. Wilson, J.D. Feikes, A.B. Zavatsky, and J.J. O'Connor. The components of passive knee movement are coupled to flexion angle. *Journal of Biomechanics*, 33(4):465 – 473, 2000.

[31] D.R. Wilson, Feikes J.D., and J.J. O'Connor. Ligaments and articular contact guide passive knee flexion. *Journal of Biomechanics*, 31:1127–1136, 1998.

[32] D.R. Wilson and J.J. O'Connor. A three-dimensional geometric model of the knee for the study of joint forces in gate. *Gait and Posture*, 5:108–115, 1997.

[33] Julius Wolff. *The Law of Bone Remodelling*. (translated into English by P. Maquet and R. Furlong). Springer Verlag, Berlin., 1986.

[34] M.-M. Yau and S.N. Srihari. A hierarchical data structure for multidimensional digital images. *Communications of the ACM*, 26(7):504 – 15, 1983.